Received: 18 January 2023 | Revised: 13 March 2023 | Accepted: 23 March 2023

DOI: 10.1002/gj.4751

RESEARCH ARTICLE

WILEY

A zircon classification scheme for sedimentary provenance analysis using radiation damage

Guanzhong Shi[1,2,3] | Chuanbo Shen[1,2] | Bastian Wauschkuhn[3] | Birk Härtel[3] | Lothar Ratschbacher[3] | Bin Xia[4] | Xiang Ge[1,2] | Xiaowei Zeng[2,5] | Hongyang Fu[2,3]

[1]Key Laboratory of Tectonics and Petroleum Resources, Ministry of Education, China University of Geosciences, Wuhan, China

[2]Faculty of Earth Resources, China University of Geosciences, Wuhan, China

[3]Geologie, TU Bergakademie Freiberg, Freiberg, Germany

[4]State Key Laboratory of Geological Processes and Mineral Resources, School of Earth Sciences, China University of Geosciences, Wuhan, China

[5]Department of Earth and Environmental Sciences, University of Milano-Bicocca, Milan, Italy

Correspondence
Guanzhong Shi, Key Laboratory of Tectonics and Petroleum Resources, Ministry of Education, China University of Geosciences, Wuhan 430074, China.
Email: cugshi@163.com

Funding information
Natural Science Foundation of Hubei Province, Grant/Award Number: 2021CFA031; National Natural Science Foundation of China, Grant/Award Numbers: 41972152, 42172182

Handling Editor: T. Tsujimori

Detrital single-grain zircon U–Pb geochronology is a powerful tool for provenance studies if information on the source rocks is available. This paper proposes a new source-rock classification tool that uses the degree of annealing of radiation damage in detrital zircon; the annealing is expressed by the relationship between the width (full-width at half-maximum; FWHM) of the $\nu_3[SiO_4]$ Raman band at ~1008 cm^{-1} and the calculated α-dose. The host rocks of the zircons are classified into three types according to their emplacement process and/or thermal history: volcanic and rapidly cooled plutonic and high-grade metamorphic rocks (type 1); rocks with hydrothermal zircons (type 2); slowly cooled igneous and metamorphic rocks (type 3). We construct a naive Bayes prediction model by training it with a collection of zircons of known types. The unknown zircons are assigned a probability of derivation from a specific host-rock type. This classification scheme is best used as an accessory tool in provenance studies that apply detrital zircon U–Pb geochronology.

KEYWORDS
annealing, Bayesian probability, provenance analysis, radiation damage, zircon classification

1 | INTRODUCTION

Detrital zircon U–Pb dating is frequently used in sediment provenance analysis because of the resistance of zircon to weathering, transport, and metamorphism (Balan et al., 2001; Feng et al., 2021; Spencer et al., 2016; Zimmermann et al., 2018). The interpretative power of provenance studies greatly depends on the comparison with the age signature of the potential source rocks. If the zircons yield broad and partially overlapping age spectra or underwent multi-stage recycling, this method is ineffective or may lead to misleading interpretations (Anderson et al., 2016; Azdimousa et al., 2019; Gehrels, 2014). Uncertainty also arises from zircon fertility; zircon-rich rocks provide an amplified age signal, while the signal from zircon-poor rocks is suppressed (e.g., Zimmermann et al., 2015).

Extracting other information from single zircons and identifying their host-rock lithologies is a possible solution (Harley et al., 2007). Owing to the α-decay of U and Th, the zircon crystal lattice is increasingly damaged up to an amorphous state (Chakoumakos et al., 1987; Holland & Gottfried, 1955). The crystalline structure is restored by annealing at high temperatures (e.g., Ende et al., 2021; Geisler, 2002;

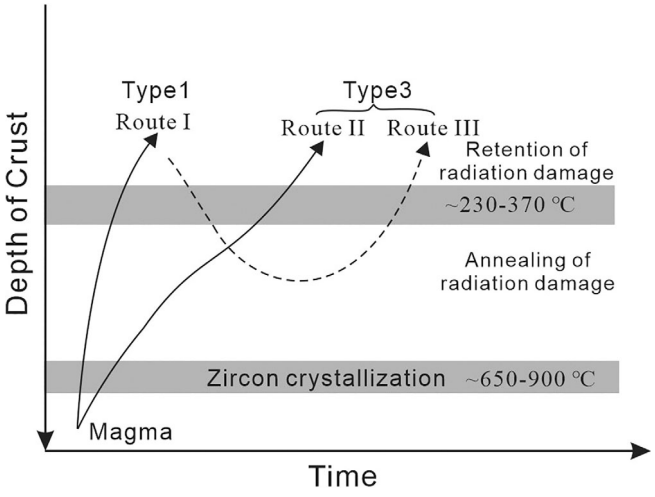

FIGURE 1 Schematic diagram showing the different emplacement routes of rocks and the temperature range of zircon crystallization and annealing. Route I: rocks cooling at high rates (e.g., volcanic rocks) rapidly pass through the temperature range of zircon crystallization and radiation-damage annealing (Härtel, Jonckheere, Wauschkuhn, Hofmann, et al., 2021; Härtel, Jonckheere, Wauschkuhn, & Ratschbacher, 2021; Pidgeon, 2014). Route II: rocks being slowly exhumed reside a prolonged time in the temperature range between zircon crystallization and annealing, e.g., rocks of a granitic batholith. Route III: rocks undergo low- to medium-grade metamorphism in the temperature range between zircon crystallization and annealing, before being exhumed to the surface (e.g., greenschist-facies rocks). This study classifies the rocks of Route I as type 1 and the rocks of Route II and III as type 3.

Geisler et al., 2001; Ginster et al., 2019; Zhang et al., 2000). The accumulated radiation damage in a zircon is a function of the U and Th concentrations, time, and the thermal history (Nasdala et al., 1998, 2001). In general, rocks exposed at the Earth's surface show thermal histories that depend on their emplacement and exhumation. The thermal history can—at least in part—be reconstructed in zircon by the degree of radiation damage (e.g., Bjerga et al., 2022; Marsellos & Garver, 2010). Thus, the petrogenetic information derived from the zircon radiation damage can enhance the database used for provenance studies and support their interpretation. This study developed a classification scheme based on zircon radiation damage density, which assigns probabilities to it being the result of rapid or slow cooling histories. To test the effect of our classification, we re-analysed detrital zircon data from Lower Cretaceous sandstones in South Africa and compared the results with the original study.

2 | CLASSIFICATION PRINCIPLES AND DATABASE

2.1 | $v_3[SiO_4]$ Raman-band vs. α-dose classifier

The classifier is based on the measured radiation damage of a zircon and the α-dose it accumulated over its lifetime. The recorded damage depends on the zircon's crystallization age and its thermal history (Härtel, Jonckheere, Wauschkuhn, Hofmann, et al., 2021). Radiation damage can be quantified by the full-width at half-maximum (FWHM) of the $v_3[SiO_4]$ Raman band (Nasdala et al., 1998, 2001). The accumulated α-dose can be calculated based on the U and Th contents and the age of the zircon (e.g., Holland & Gottfried, 1955; Murakami et al., 1991; Nasdala et al., 2001). The empirical relationship between the α-dose and FWHM is given by Váczi and Váczi and Nasdala (2017) as:

$$\mathrm{FWHM} = 34.96\left[\mathrm{cm}^{-1}\right] - 33.16\left[\mathrm{cm}^{-1}\right]\exp\left(-5.32 \times 10^{-19}[g/\alpha]D_{\alpha}\right) \quad (1)$$

where D_{α} is the calculated α-dose. This equation gives the FWHM in case of lacking lattice repair by annealing.

When a rock is rapidly exhumed to the Earth's surface after crystallization (Figure 1, Route I), little annealing occurs and α-damage in zircon is retained; zircons from such rocks cluster along an empirically-determined exponential line, which traces the Radiation-Damage Accumulation Path in a graph of α-dose versus FWHM (Figure 2a). In nature, rapidly cooled rocks are volcanics and small-volume plutonic rocks that were emplaced in the upper (cold) crust. Such rocks cool so rapidly that nearly all radiation damage is preserved within the zircons. We classify such rocks as type 1 (Table 1).

In many high-grade metamorphic rocks, zircons recrystallize and thus experience a reset of the U–Pb isotopic system. Such zircons undergo a complete repair of radiation damage and only accumulate new damage after cooling through the temperature range in which annealing occurs (see below; Härtel, Jonckheere, Wauschkuhn, & Ratschbacher, 2021). When these high-grade metamorphic rocks are rapidly exhumed through this radiation-damage annealing zone, the high cooling rate prevents significant annealing. We classify such rocks as type 1 as well (Table 1); they also plot along the Radiation-Damage Accumulation Path (Figure 2a). In our training data set (see below), zircons from the Bohemian-Massif granulites (Sláma et al., 2008; Tichomirowa et al., 2005) represent such type 1 high-grade metamorphic host rocks (Figure 2a). These granulites exhumed at a rate of ~4 km/Ma and cooled at ~20–50°C/Ma (Kotková, 2007).

Damage annealing in zircon occurs at temperatures higher than 230–370°C (e.g., Härtel, Jonckheere, Wauschkuhn, & Ratschbacher, 2021; Pidgeon, 2014) and restores its crystallinity. In nature, zircon annealing is related to: (1) slow cooling that follows crystal formation (Figure 1, Route II) with prolonged retention at elevated temperatures (e.g., Pidgeon, 2014), such as it is the case in large-volume granitoid bodies intruding into the middle and lower crust; and (2) reheating to elevated temperatures over geological time in the course of low- to medium-grade metamorphism (Figure 1, Route III). Greenschist- to amphibolite-facies metamorphism involves temperatures between 300 and 650°C (e.g., Willner et al., 2018). In this case, annealing reduces the FWHM, depending on the temperature–time conditions of the rock (Marsellos & Garver, 2010). Zircons that underwent annealing because of slow exhumation/

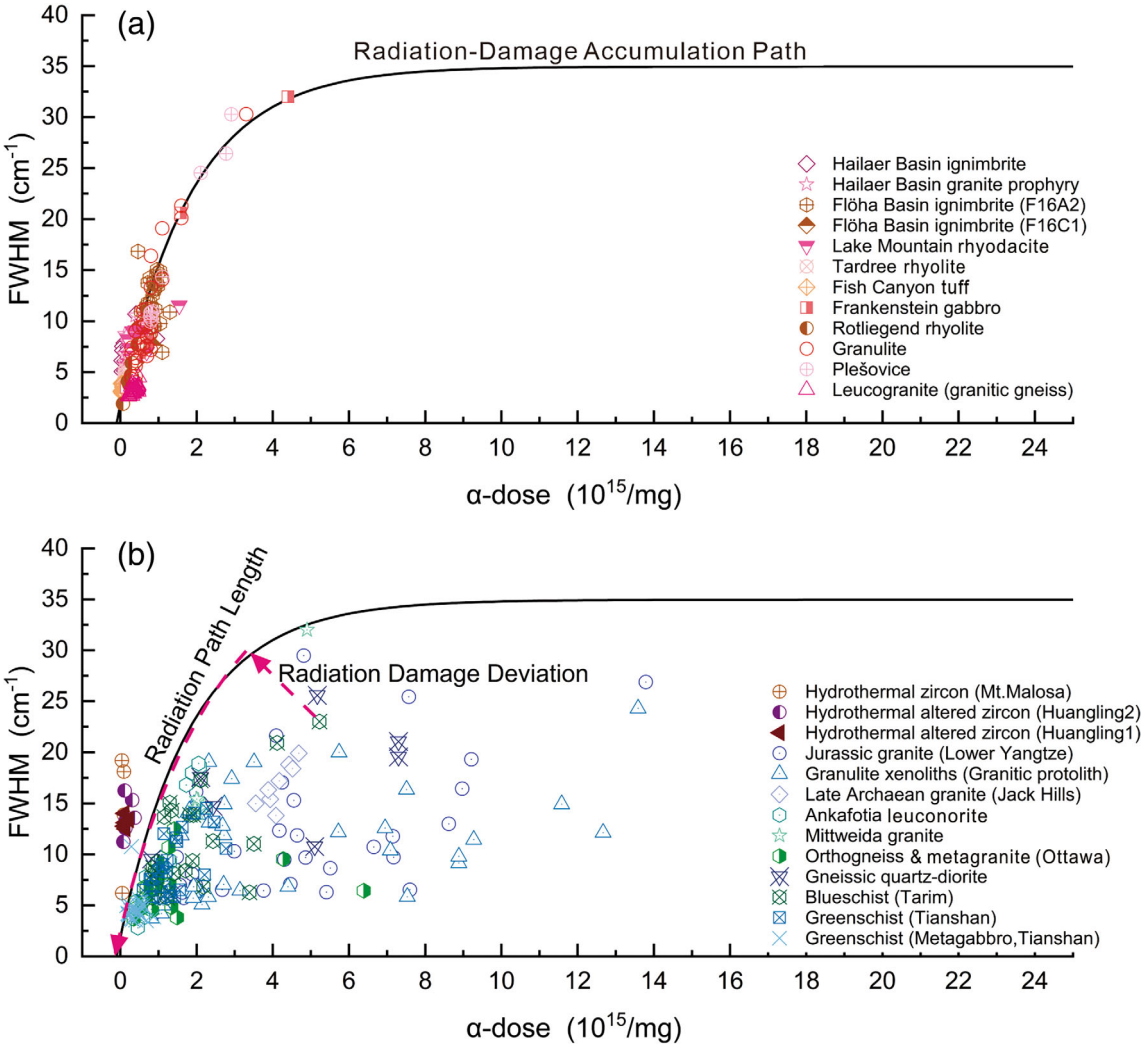

FIGURE 2 Plots of α-dose versus full-width at half-maximum (FWHM) for zircons of different rock types. The lossless radiation-damage accumulation path refers to equation (2) in Váczi and Nasdala (2017) that assumes FWHM = 1.8 cm^{-1} at zero α-dose based on synthetic zircon. (a) Zircons of type 1 rocks follow closely the radiation-damage accumulation path. (b) Zircons of type 2 (hydrothermal zircons) and type 3 are offset from the radiation-damage accumulation path. References for the plotted data are listed in Appendix S1. Red dashed arrows define the Radiation Damage Deviation and Radiation Path Length that are the two parameters characterizing the differences between zircons.

TABLE 1 List of major types of zircon source rocks and the number of grains.

Type	Lithology	Number
1	Rapidly cooled volcanic rocks, igneous bodies of small volume, high/ultra-high pressure metamorphic rocks in orogenic belts.	237
2	Zircons precipitated from or overprinted by hydrothermal fluids.	16
3	Slowly cooled granitoids, basement rocks of granulitic- to amphibolitic-grade metamorphism in which the U–Pb system was reset, low- to medium-grade metamorphic rocks	230

cooling or reheating thus plot below the Radiation-Damage Accumulation Path; such thermal histories (type 3) are typical for granitic batholiths and medium- and low-grade metamorphic rocks (Figure 2b).

Hydrothermal zircons (type 2) generally deviate from the accumulation trend at a very low α-dose (Figure 2b). This means that the damage inferred from the FWHM exceeds the theoretical damage ascribed to a maximal possible radioactive α-dose. The high FWHM is because of significant band asymmetry, likely resulting from substitution-related strain and disorder (Kempe et al., 2018). The band asymmetry is alternatively explained by damage heterogeneity within a single analysis spot because of a contrasting distribution of actinide elements in zircons (Härtel et al., 2022; Nasdala et al., 2005). The very low α-dose of hydrothermal zircons is related to the low concentrations of Th and U compared with most magmatic zircons, because such zircons experience migration of U and Th because of fluid activity (Schaltegger, 2007; Tichomirowa et al., 2005).

2.2 | Analytical method and database

A zircon database (483 grains, Table 1) was compiled from the literature and covers igneous and metamorphic rocks from different parts of the world (Appendix S1). The α-dose was calculated according to the U–Pb ages and the U and Th concentrations. The compiled zircon U–Pb ages, U and Th concentrations, and Raman spectroscopic data are from single grains of known host-rock type. For zircons with complex structures (e.g., core–mantle-rim), the U–Pb ages, U and Th concentrations, and Raman measurements are from the same spot. Zircons with discordant U–Pb ages (e.g., zircons outside the range of 90%–110% concordance in the $^{238}U/^{206}Pb$ and $^{206}Pb/^{207}Pb$ ages) and heterogeneous grains that show large variations of FWHM and Raman shift within a single zircon were removed (e.g., Härtel et al., 2022). The collected bandwidths were recalculated for the instrumental profile function (IPF) following Váczi (2014). The corrected bandwidth data may bear uncertainties owing to different instrument conditions. However, these uncertainties merely influence the variance in the classifier and would not significantly bias the mathematical mean value and the final statistical results (i.e., probability value; see below).

We also included new data from (1) Cretaceous volcanics of the Hailaer Basin, NE China, (2) Neoproterozoic granitic gneisses of the Huangling massif, northwestern Yangtze Craton, that contain hydrothermally-altered zircons, (3) Neoproterozoic blueschists from the Akesu area in Tarim, NW China (metamorphism at ~805 Ma), and (4) Late Palaeozoic greenschists from southwestern Tian Shan, NW China (metamorphism at 310–320 Ma; Xia et al., 2014, 2016, 2019). The Raman spectra were analysed in the Key Laboratory of Tectonics and Petroleum Resources, China University of Geosciences, Wuhan. The JY/Horiba Labram HR800 Raman system is equipped with a frequency doubled Nd:YAG laser (532.06 nm, 20 mW at the sample surface) with a laser power of 25 mW and a long-working-distance Olympus objective with a 0.5 numerical aperture. The lateral resolution was ~1.5 μm and the depth resolution was ~2 μm. Raman peak-position calibration was verified regularly with the ~520.7 cm^{-1} band of a polished silicon wafer before the measurement. We used a high-resolution grating (1800 g mm^{-1}) and a narrow slit (50 μm) for peak-resolution increase. The proximate spectral resolution is ~0.8 cm^{-1}. Raman bands were fitted using the Voigt function of the Origin® (v. 2018) software that can automatically work out the FWHM and peak centers of the $v_3(SiO_4)$ band. Because the FWHM of the fitted profile is sensitive to the exact form of the baseline, the same type of baseline (hyperbolic) was used for all the spectra. The bandwidth correction for the IPF follows Váczi (2014).

3 | PARAMETER CALCULATION AND MODEL CONSTRUCTION

3.1 | Parameter settings

Two parameters were defined to maximize the differences between the zircons in the classifier. *Radiation Damage Deviation* is the shortest distance from a given point in the damage (FWHM) versus α-dose diagram to the Radiation Damage Accumulation Path (Figure 2b); it describes the degree of annealing. *Radiation Path Length* is the curve length from the projection of a given point onto the Path to the zero-damage point (Figure 2b). Here, we do not directly use the FWHM value to quantify the degree of annealing, because the annealing process causes the FWHM value (i.e., *y*-axis) to gradually decrease with the accumulation of the α-dose (i.e., *x*-axis in Figure 2), which is a curve that has a smaller radius of curvature than the Radiation Damage Accumulation Path. The advantage of using the proposed two parameters, rather than the FWHM (i.e., *y*-value) and α-dose (i.e., *x*-value), is that they approximate the real annealing path while maximizing the annealing difference between each zircon. All training zircons were computed in the form of the Radiation Path Length and Radiation Damage Deviation to obtain the mean value and variance for each zircon type (types 1–3, see above). Then, the unknown zircons were compared with the mathematical means of the types 1–3 to get the relative distances to each zircon type; the closer the distance the higher the likelihood that an unknown zircon belongs to a certain zircon type and thus gives a higher probability value. Kernel density statistics shows that type 1 and type 2 rocks can be better discriminated by the Radiation Damage Deviation, whereas type 3 slightly overlaps with type 1 (Figure 3). The slight overlap is because of the existence of zircons of low α-dose and low FWHM values (Figure 2b).

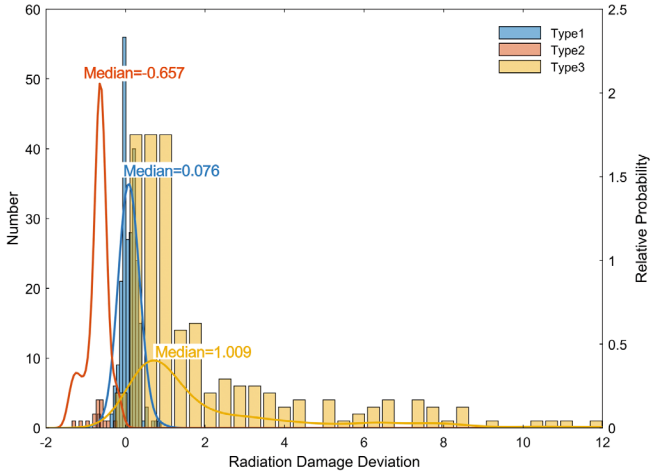

FIGURE 3 Histograms and Kernel density estimates of zircons of types 1–3 based on the Radiation Damage Deviation parameter. The overlap between type 1 and type 3 is partly related to low α-dose zircons (particularly the metagabbro in Figure 2) that lead to a potential classification error.

Bayes theory is of great importance to the processing of prior information so as to form a prior distribution for statistical inference (Blanquero et al., 2021; Kim et al., 2020). The prior distribution reflects the proportion of each zircon type (i.e., prior probability), and in our case, the prior probabilities can be viewed as the potential proportions of each zircon type derived from a specific source area. The Bayes algorithm gives a posterior probability to the unknown zircons, assuming that each type of zircon has equal chance to occur; the final

TABLE 2 The confusion matrix of zircon training and prediction.

	Predicted zircon type								
	Posterior probabilities[a]			Prior probabilities[b]			Prior probabilities[b]		
	Type 1	Type 2	Type 3	Type 1	Type 2	Type 3	Type 1	Type 2	Type 3
Trained zircon type									
Type 1	226	4	7	227	1	9	220	1	16
Type 2	1	15	0	1	15	0	1	15	0
Type 3	42	0	188	43	0	187	34	0	196

[a]Posterior probability is calculated assuming that each zircon type has equal weight.
[b]Calculated according to prior probabilities of the frequency of training zircons and the global prior estimates, respectively.

probability is obtained through a weighted calculation by the prior value. The prior probabilities act as a perturbation to intervene the final probability. This study uses the frequency of training zircons as the prior probability, and we also recommend a global prior probability, which refers to the proportions of global lithologies and zircon fertility, that is, the abundance of zircons in different rocks (Dürr et al., 2005, Appendix S2). Users can assign their own values of prior probability according to the lithologic proportions when studying a particular geological area.

3.2 | Model construction and validation test

The model construction uses the package "Naive Bayes" for MATLAB (MathWorks version 2016); details about the codes are in Appendix S4. The classifier gives posterior and prior weighted probability estimates of a zircon belonging to a certain rock type. Table 2 shows the confusion matrices. Most errors come from type 3 zircons; some are misclassified as type 1. The 10-fold cross-validation tests suggest a 95% confidence for a correct classification when removing inherited zircons from the type 1 class and low-damage zircon from the type 3 class (Appendix S2, details in the next section).

We used a published provenance study, investigating Lower Cretaceous sandstones from South Africa (Resentini et al., 2020, Appendix S3), to validate our method. The samples of South Africa were divided into five age populations (at ~120, ~270, 350–760, 760–1400, and 1400–2200 Ma). We assigned priors of 0.28, 0.10, 0.62 to the types 1–3 classes, respectively, which slightly deviate from the global priors. The prior values were estimated based on the following reasons: (i) petrographic studies suggest that volcanic, granitic, and metamorphic rocks contributed to the zircon populations of the sedimentary rocks, and (ii) the potential source areas are dominated by cratonic basement rocks and granitoids. Our analysis results are comparable with the results of the original study in a way that all the "annealed" grains are predicted as type 3, and most of the Precambrian zircons are classified as granitoids and basement rocks, in agreement with the great volume of outcropping cratonic basement rocks and their "multiple-annealed" nature, as suggested by the original study. The inconsistent results come from the "unannealed" zircons: 51 of 82 grains that were identified as "unannealed" zircons in the original study are predicted as type 3 (i.e., annealed zircon) by our method (Appendix S3). These contrasting predictions relate to the different thresholds assigned to the annealed and unannealed zircons. This study defines the annealed/unannealed threshold by training zircons of known thermal histories, whereas Resentini et al. (2020) classified zircons by an iterative mathematical calculation, based on ages that have experienced an assumed thermal history, although these ages have relative uncertainties of ±10%.

4 | DISCUSSION AND EVALUATION

4.1 | Sources of classification errors

The classification errors mainly come from low-damage zircons (FWHM <8 cm^{-1}, α-dose <0.46 × 10^{15} α/mg; Ginster et al., 2019, Figure 4). These low-damage zircons are misclassified as type 1 or type 3 (Table 2). There might be a threshold α-dose before radiation damage is reflected in the $v_3[SiO_4]$ Raman band (Jonckheere et al., 2019), although we cannot exclude that the errors are related to the high relative errors of the α-dose calculations and the Raman measurements on the low-damage zircons. The classifier is not sensitive to the FWHM variations of low α-dose grains (e.g., metagabbro-derived zircons), and thus low radiation-damage zircons of type 3 can be misclassified as type 1. Another error source are inherited zircons in volcanic rocks that violate the relationship between radiation damage and cooling rate (Figure 4). These inherited zircons record a higher α-dose because of their older U–Pb ages than the zircons crystallized in the volcanic rocks, but underwent high-T annealing in the melt, and thus are plotted in the field of type 3; this deviation from the Radiation Damage Accumulation Path was used to identify inherited zircon in volcanic rocks (Bjerga et al., 2022). In practice, inherited zircons are classified as type 3, which directly points to the original rocks while ignoring the volcanic capture. In contrast, inherited zircons in igneous plutons are classified as type 3, which is the correct classification. These inherited zircons have older U–Pb ages than their host plutons and thus have higher calculated α-dose values; these shift them towards the type 3 field.

Zircon Raman analysis usually measures one or a few points on a polished surface; obviously such measurements are not representative

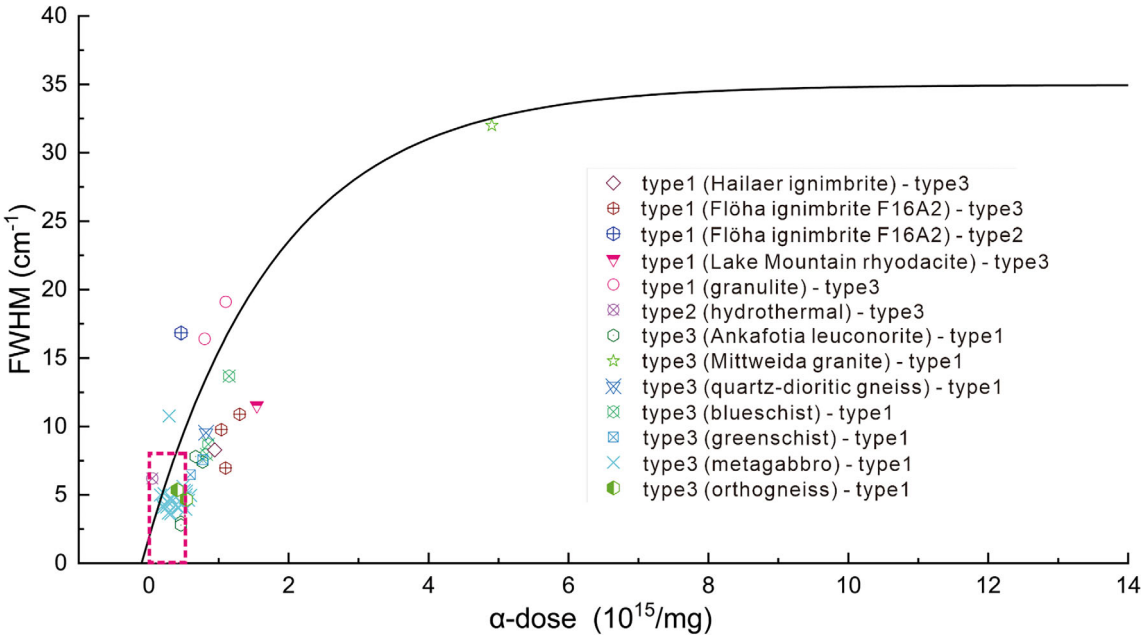

FIGURE 4 Distribution of the misclassified zircons. In the legend, the zircon types before and after the dash (–) are the true types and the incorrect identifications, respectively. The red dotted box encloses the low-damage zircons (FWHM <8 cm^{-1}, α-dose <0.46 × 10^{15} α/mg, Ginster et al., 2019), for example, the metagabbro-derived grains that are a major source of classification error. Another error source are the outliers in the training set (e.g., from ignimbrites and rhyodacites), which lie off the accumulation path and are assigned to type 3. Table 2 details the number of misclassifications.

for zircon with complex structures (e.g., core-rim structures). Although these complex structures also cause classification bias, such zircon is relatively rare in sedimentary rocks. The proposed classification scheme is mainly for zircon with simple structure that accounts for the majority in sedimentary rocks.

4.2 | Influence of priors

The confusion matrices and the visual diagrams show the classification effect and the influence of the prior probability (Table 2, Figure 5). The posterior probabilities suggest that most type 1 zircons are predicted as type 1 ones; a small number of zircons are identified as type 3 and type 2 (Figure 5a). After the weighted calculation by the frequency of the training zircons, the relatively high weight of type 1 zircons renders the predicted results to shift slightly towards the type 1 area; this improves the accuracy from 95.3% to 95.7%. By contrast, the overestimated weight of type 3 zircons in the global priors causes the predicted results to migrate towards type 3 ones, reducing the accuracy from 95.3% to 92.8% (Figure 5a). Similar variations occur in the predictions of type 2 and type 3 zircons (Figure 5b,c). An underestimation or overestimation of the weight for a certain type of zircon results in a corresponding change in the final probability. However, this will cause a change in the classification only if the probability value crosses the 0.5 threshold, it will cause a change in the classification. This means that when the relationship between the Raman FWHM and the α-dose strongly suggests a particular cooling history and thus indicates a certain host rock, the prior probabilities have no influence on the final discriminant results. For example, in the type 2 prediction, the grains of posterior probabilities >0.9 are influenced by the prior probabilities but are not wrongly classified as other types (Figure 5b). On the other hand, when the discriminant fails to offer compelling posterior probabilities in favour of any provenance, prior probabilities are helpful to obtain a better estimate. For example, in the type 3 prediction, only the grains of posterior probabilities close to 0.5 can be influenced by the prior probabilities and eventually can change the classification (Figure 5c).

4.3 | Instruction of use

One should be cautious with low α-dose zircons (<0.46 × 10^{15} α/mg). Low α-dose zircons cannot have large deviations from the accumulation trend, and the parameters of the Raman instrument used might render variations in FWHM imperceptible, resulting in a misclassification. In practice, we recommend two alternative ways to strengthen the credibility of the classification: (i) removing low-damage zircons (<0.46 × 10^{15} α/mg or FWHM<8 cm^{-1}) and using high-damage zircons to predict the host-rock type; or (ii) using zircons with high probability values, for example 0.7, as a threshold to determine the host-rock types. Most errors come from zircons with a probability value close to 0.5, as in the case of low-damage zircons. In other words, the use of high-damage zircon is sufficient for the task of predicting the host-rock types and thus indicating the sources.

The validity of classification scheme relies on the number of zircons used for training the classification. The range of each zircon type greatly depends on the delineation of a large number of zircons. Currently, however, the number of training zircons is relatively small,

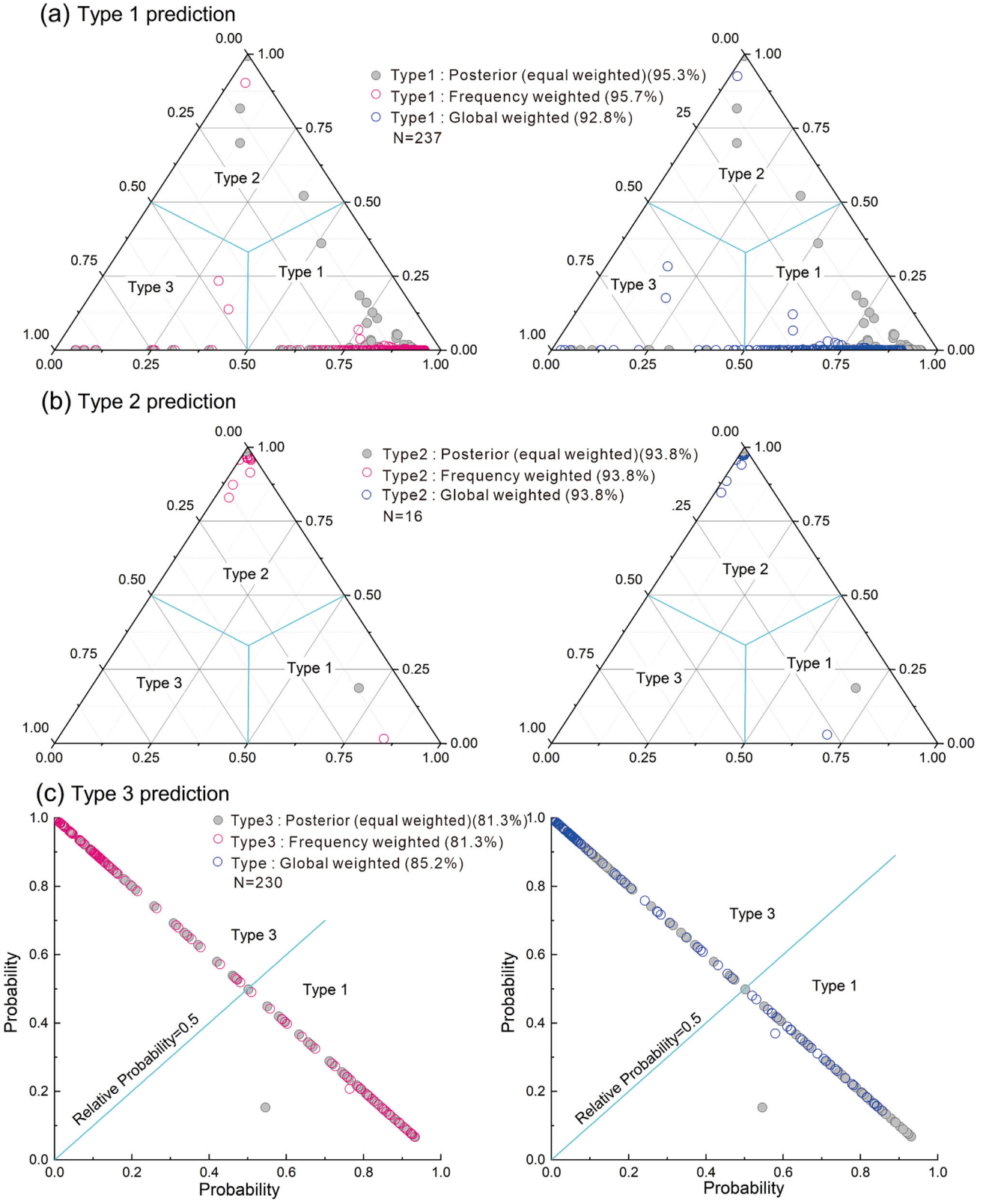

FIGURE 5 Ternary and binary diagrams of the probabilities obtained for the relevant host-rock types. (a), (b), and (c) show the influences of prior probabilities on the determination of zircons from volcanics and exhumed granulites (type 1), hydrothermal zircons (type 2), and zircons from granitoids and metamorphic rocks (type 3), respectively. The coordinate axes represent probabilities ranging from 0 to 1. The blue lines outline the range of each type. Probabilities of posterior, frequency of training zircons (type 1: type 2: type 3 = 0.491:0.033:0.476), and global priors (type 1: type 2: type 3 = 0.291:0.046:0.663) are compared with the labelled accuracy. The predicted probabilities of type 3 grains as being type 2 are close to zero and thus the use of binary diagram (c) better illustrates the effect of the prior probabilities.

particularly for hydrothermal zircon, for which the published database is limited. It is conceivable that some hydrothermal zircon may be misidentified as type 1 (e.g., volcanic zircon) or type 3 (e.g., zircon from slowly cooled granitoids). We suggest that additional information (e.g., zircon textures, trace elements) shall be taken into account when using the classifier in the current version to identify hydrothermal zircon. The classifier can be improved by continually adding more known types of zircon from around the globe and/or training known types of zircon from user research areas.

Priors are only helpful to distinguish zircon types when the posterior probabilities are close to 0.5. Users can set their own prior probabilities for a particular area and a specific era. Suggestions for setting prior probabilities are: (i) use of age spectra from detrital zircons, because a particular age peak usually represents a distinct geological event or a combination of several similar-aged geological events. For example, the zircons of the ~120 Ma peak in the South Africa dataset represent the rift-related magmatism and zircons of the ~560 Ma peak represent the magmatic and metamorphic events of the Zambezi orogenic belt (Kuribara et al., 2019); (ii) considering petrographic information of clastic rocks; this provides the most direct constraints for priors.

5 | CONCLUSIONS

Radiation damage in zircon caused by α-decay of U and Th accumulates following crystallization and is repaired at elevated temperatures. This study assumes that the degree of radiation damage in zircons is genetically related to the thermal history of their host rocks. Volcanic extrusions and granitic intrusions usually have contrasting cooling rates and thermal overprints usually occur because of metamorphism. These assumptions are the theoretical basis for distinguishing zircon types in sedimentary rocks by their degree of radiation damage. This study develops a classification scheme using the α-dose versus damage FWHM diagram and divides natural zircons into three types: (1) rapidly cooled, (2) hydrothermal, and (3) slowly cooled or reheated. A naive Bayes classifier is established using compiled zircon age and Raman data that displays a good performance with low classification errors.

AUTHOR CONTRIBUTIONS

Guanzhong Shi: Conceptualization, Formal analysis, Funding acquisition, Project administration, Visualization, validation, Writing-original draft. **Chuanbo Shen:** Funding acquisition, Supervision, Writing-Review & Editing. **Bastian Wauschkuhn:** Conceptualization, Sample resources, Writing-review & editing. **Birk Härtel:** Conceptualization, Sample resources, Data curation, Writing-review & editing. **Lothar Ratschbacher:** Conceptualization, Writing-review & editing. **Xia Bin:** Sample resources. **Xiang Ge:** Formal analysis. **Xiaowei Zeng:** Formal analysis. **Hongyang Fu:** Formal analysis.

ACKNOWLEDGEMENTS

This study was financed by the Innovation Team Project of the Natural Science Foundation of Hubei Province (No. 2021CFA031) and the National Natural Science Foundation of China (Nos. 42172182, 41972152). Open Access funding enabled and organized by Projekt DEAL.

PEER REVIEW

The peer review history for this article is available at https://www.webofscience.com/api/gateway/wos/peer-review/10.1002/gj.4751.

DATA AVAILABILITY STATEMENT

The data that supports the findings of this study are available in the supplementary material of this article.

REFERENCES

Anderson, T., Kristoffersen, M., & Elburg, M. (2016). How far can we trust provenance and crustal evolution information from detrital zircons? A south African case study. *Gondwana Research*, *34*, 129–148.

Azdimousa, A., Jabaloy-Sánchez, A., Talavera, C., Asebriy, L., González-Lodeiro, F., & Evans, N. J. (2019). Detrital zircon U-Pb ages in the Rif Belt (northern Morocco): Paleogeographic implications. *Gondwana Research*, *70*, 133–150.

Balan, E., Neuville, D. R., Trocellier, P., Fritsch, E., Muller, J. P., & Calas, G. (2001). Metamictization and chemical durability of detrital zircon. *American Mineralogist*, *86*, 1025–1033.

Bjerga, A., Stubseid, H. H., Pedersen, L. E. R., & Pedersen, R. B. (2022). Radiation damage allows identification of truly inherited zircon. *Communications Earth & Environment*, *3*(37), 1–7.

Blanquero, R., Carrizosa, E., Ramírez-Cobo, P., & Sillero-Denamiel, M. R. (2021). Variable selection for Naïve Bayes classification. *Computers & Operations Research*, *135*, 105456.

Chakoumakos, B. C., Murakami, T., Lumpkin, G. R., & Ewing, R. C. (1987). Alpha-decay—Induced fracturing in zircon: The transition from the crystalline to the metamict state. *Science*, *236*(4808), 1556–1559.

Dürr, H. H., Meybeck, M., & Dürr, S. H. (2005). Lithologic composition of the Earth's continental surfaces derived from a new digital map emphasizing riverine material transfer. *Global Biogeochemical Cycles*, *19*(4), GBS4S10.

Ende, M., Chanmuang, N. C., Reiners, P. W., Zamyatin, D. A., Gain, S. E. M., Wirth, R., & Nasdala, L. (2021). Dry annealing of radiation-damaged zircon: Single-crystal X-ray and Raman spectroscopy study. *Lithos*, *406-407*, 106523.

Feng, Y., Song, C. H., He, P. J., Meng, Q. Q., Wang, Q. X., Wang, X. H., & Chen, W. Q. (2021). Detrital zircon U-Pb geochronology of the Jianchuan Basin, southeastern Tibetan plateau, and its implications for tectonic and paleodrainage evolution. *Terra Nova*, *33*(6), 560–572.

Gehrels, G. (2014). Detrital zircon U-Pb geochronology applied to tectonics. *Annual Review of Earth and Planetary Sciences*, *42*, 127–149.

Geisler, T. (2002). Isothermal annealing of partially metamict zircon: Evidence for a three-stage recovery process. *Physics and Chemistry of Minerals*, *29*, 420–429.

Geisler, T., Pidgeon, R. T., van Bronswijk, W., & Pleysier, R. (2001). Kinetics of thermal recovery and recystallisation of partially metamict zircon: A Raman spectroscopic study. *European Journal of Mineralogy*, *13*, 1163–1176.

Ginster, U., Reiners, P. W., Nasdala, L., & Chutimun, C. N. (2019). Annealing kinetics of radiation damage in zircon. *Geochimica et Cosmochimica Acta*, *249*, 225–246.

Harley, S. L., Kelly, N. M., & Moller, A. (2007). Zircon behavior and the thermal histories of mountain chains. *Elements*, *3*, 25–30.

Härtel, B., Jonckheere, R., & Ratschbacher, L. (2022). Multi-band Raman analysis of radiation damage in zircon for thermochronology: Partial annealing and mixed signals. *Geochemistry, Geophysics, Geosystems*, *23*, e2021GC010182. https://doi.org/10.1029/2021GC010182

Härtel, B., Jonckheere, R., Wauschkuhn, B., Hofmann, M., Frölich, S., & Ratschbacher, L. (2021). Zircon Raman dating: Age equation and calibration. *Chemical Geology*, *579*, 120351.

Härtel, B., Jonckheere, R., Wauschkuhn, B., & Ratschbacher, L. (2021). The closure temperature(s) of zircon Raman dating. *Geochronology*, *3*, 259–272.

Holland, H. D., & Gottfried, D. (1955). The effect of nuclear radiation on the structure of zircon. *Acta Crystallographica*, *8*, 291–300.

Jonckheere, R., Heinz, D., Hacker, B. R., Rafaja, D., & Ratschbacher, L. (2019). A borehole investigation of zircon radiation damage annealing. *Terra Nova*, *31*, 263–270.

Kempe, U., Trullenque, G., Thomas, R., Sergeev, S., Presnyakov, S., Rodionov, N., & Himcinschi, C. (2018). Substitution-induced internal strain and high disorder in weakly radiation damaged hydrothermal zircon from Mt. Malosa, Malawi. *European Journal of Mineralogy*, *30*, 659–679.

Kim, H. C., Park, J. H., Kim, D. W., & Lee, J. (2020). Multilabel naïve Bayes classification considering label dependence. *Pattern Recognition Letters*, *136*, 279–285.

Kotková, J. (2007). High-pressure granulites of the bohemian massif: Recent advances and open questions. *Journal of Geosciences*, *52*(1–2), 45–71.

Kuribara, Y., Tsunogae, T., Takamura, Y., & Tsutsumi, Y. (2019). Petrology, geochemistry, and zircon U-Pb geochronology of the Zambezi Belt in Zimbabwe: Implications for terrane assembly in southern Africa. *Geoscience Frontiers*, *10*(6), 2021–2044.

Marsellos, A. E., & Garver, J. I. (2010). Radiation damage and uranium concentration in zircon as assessed by Raman spectroscopy and neutron irradiation. *American Mineralogist*, *95*(8–9), 1192–1201.

Murakami, T., Chakoumakos, B. C., Ewing, R. C., Lumpkin, G. R., & Weber, W. J. (1991). Alpha-decay damage in zircon. *American Mineralogist*, *76*, 1510–1532.

Nasdala, L., Hanchar, J. M., Kronz, A., & Whitehouse, M. J. (2005). Long-term stability of alpha particle damage in natural zircon. *Chemical Geology*, *220*, 83–103.

Nasdala, L., Pidgeon, R. T., Wolf, D., & Irmer, G. (1998). Metamictization and U-Pb isotopic discordance in single zircons: A combined Raman microprobe and SHRIMP ion probe study. *Mineralogy and Petrology*, *62*, 1–27.

Nasdala, L., Wenzel, M., Vavra, G., Irmer, G., Wenzel, T., & Kober, B. (2001). Metamictisation of natural zircon: Accumulation versus thermal annealing of radioactivity-induced damage. *Contribution to Mineralogy and Petrology*, *141*, 125–144.

Pidgeon, R. T. (2014). Zircon radiation damage ages. *Chemical Geology*, *367*, 13–22.

Resentini, A., Andò, S., Garzanti, E., Malusà, M. G., Pastore, G., Vermeesch, P., Chanvry, E., & Dall'Asta, M. (2020). Zircon as a provenance tracer: Coupling Raman spectroscopy and U-Pb geochronology in source-to-sink studies. *Chemical Geology*, *555*, 119828.

Schaltegger, U. (2007). Hydrothermal zircon. *Elements*, *3*, 51–52.

Sláma, J., Košler, J., Condon, D. J., Crowley, J. L., Gerdes, A., Hanchar, J. M., Horstwood, M. S. A., Morris, G. A., Nasdala, L., Norberg, N., Schaltegger, U., Schoene, B., Tubrett, M. N., & Whitehouse, M. J. (2008). Plesovice zircon—A new natural reference material for U-Pb and Hf isotopic microanalysis. *Chemical Geology*, *249*, 1–35.

Spencer, C. J., Kirkland, C. L., & Taylor, R. J. M. (2016). Strategies towards statistically robust interpretations of in situ U–Pb zircon geochronology. *Geoscience Frontiers*, *7*(4), 581–589.

Tichomirowa, M., Whitehouse, M. J., & Nasdala, L. (2005). Resorption, growth, solid state recrystallisation, and annealing of granulite facies zircon—A case study from the Central Erzgebirge, bohemian massif. *Lithos*, *82*, 25–50.

Váczi, T. (2014). A new, simple approximation for the deconvolution of instrumental broadening in spectroscopic band profiles. *Applied Spectroscopy*, *68*(11), 1274–1278.

Váczi, T., & Nasdala, L. (2017). Electron-beam-induced annealing of natural zircon: A Raman spectroscopic study. *Physics and Chemistry of Minerals*, *44*, 389–401.

Willner, A. P., van Staal, C. R., Zagorevski, A., Glodny, J., Romer, R. L., & Sudo, M. (2018). Tectonometamorphic evolution along the Iapetus suture zone in Newfoundland: Evidence for polyphase Salinic, Acadian and Neoacadian very low- to medium-grade metamorphism and deformation. *Tectonophysics*, *742-743*, 137–167.

Xia, B., Zhang, L. F., Bader, T., Shen, T. T., & Chen, N. S. (2016). Late Palaeozoic $^{40}Ar/^{39}Ar$ ages of the HP-LT metamorphic rocks from the Kekesu Valley, Chinese southwestern Tianshan: New constraints on exhumation tectonics. *International Geology Review*, *58*(4), 389–404.

Xia, B., Zhang, L. F., Du, Z. X., & Xu, B. (2019). Petrology and age of Precambrian Aksu blueschist, NW China. *Precambrian Research*, *326*, 295–311.

Xia, B., Zhang, L. F., Xia, Y., & Bader, T. (2014). The tectonic evolution of the Tianshan Orogenic Belt: Evidence from U-Pb dating of detrital zircons from the Chinese southwestern Tianshan accretionary mélange. *Gondwana Research*, *25*, 1627–1643.

Zhang, M., Salje, E. K. H., Farnan, I., Graeme-Barber, A., Daniel, P., Ewing, R. C., Clark, A. M., & Leroux, H. (2000). Metamictization of zircon: A Raman spectroscopic study. *Journal of Physics Condensed Matter*, *12*, 1915–1925.

Zimmermann, S., Mark, C., Chew, D., & Voice, P. J. (2018). Maximising data and precision from detrital zircon U-Pb analysis by LA-ICPMS: The use of core-rim ages and the single-analysis Concordia age. *Sedimentary Geology*, *375*, 5–13.

Zimmermann, U., Anderson, T., Madland, M. V., & Larsen, I. S. (2015). The role of U-Pb ages of detrital zircons in sedimentology—An alarming case study for the impact of sampling for provenance interpretation. *Sedimentary Geology*, *320*, 38–50.

SUPPORTING INFORMATION

Additional supporting information can be found online in the Supporting Information section at the end of this article.

How to cite this article: Shi, G., Shen, C., Wauschkuhn, B., Härtel, B., Ratschbacher, L., Xia, B., Ge, X., Zeng, X., & Fu, H. (2023). A zircon classification scheme for sedimentary provenance analysis using radiation damage. *Geological Journal*, *58*(8), 3087–3095. https://doi.org/10.1002/gj.4751